Atmos. Chem. Phys. Discuss., 12, 14837–14874, 2012
www.atmos-chem-phys-discuss.net/12/14837/2012/
doi:10.5194/acpd-12-14837-2012

Atmospheric Chemistry and Physics Discussions

The impact of deforestation in the Amazonian atmospheric radiative balance: a remote sensing assessment

E. T. Sena, P. Artaxo, and A. L. Correia

Institute of Physics, University of São Paulo, São Paulo, Brazil

Received: 30 May 2012 – Accepted: 31 May 2012 – Published: 12 June 2012

Correspondence to: E. T. Sena (elisats@if.usp.br)

Published by Copernicus Publications on behalf of the European Geosciences Union.

Abstract

This paper addresses the Amazonian radiative budget after considering three aspects of deforestation: (i) the emission of aerosols from biomass burning due to forest fires; (ii) changes in surface albedo after deforestation and (iii) modifications in the column water vapour amount over deforested areas. Simultaneous Clouds and the Earth's Radiant Energy System (CERES) shortwave fluxes and aerosol optical depth (AOD) retrievals from the Moderate Resolution Imaging SpectroRadiometer (MODIS) were analysed during the peak of the biomass burning seasons (August and September) from 2000 to 2009. A discrete-ordinate radiative transfer (DISORT) code was used to extend instantaneous remote sensing radiative forcing assessments into 24-h averages.

The mean direct radiative forcing of aerosols at the top of the atmosphere (TOA) during the biomass burning season for the 10-yr studied period was $-5.6 \pm 1.7\,\mathrm{W\,m^{-2}}$. Furthermore, the spatial distribution of the direct radiative forcing of aerosols over Amazon was obtained for the biomass burning season of each year. It was observed that for high AOD (larger than 1 at 550 nm) the imbalance in the radiative forcing at the TOA may be as high as $-20\,\mathrm{W\,m^{-2}}$ locally. The surface reflectance plays a major role in the aerosol direct radiative effect. The study of the effects of biomass burning aerosols over different surface types shows that the direct radiative forcing is systematically more negative over forest than over savannah-like covered areas. Values of $-15.7 \pm 2.4\,\mathrm{W\,m^{-2}}/\tau_{550\,\mathrm{nm}}$ and $-9.3 \pm 1.7\,\mathrm{W\,m^{-2}}/\tau_{550\,\mathrm{nm}}$ were calculated for the mean daily aerosol forcing efficiencies over forest and savannah-like vegetation respectively. The overall mean annual albedo-change radiative forcing due to deforestation over the state of Rondônia, Brazil, was determined as $-7.3 \pm 0.9\,\mathrm{W\,m^{-2}}$. Biomass burning aerosols impact the radiative budget for approximately two months per year, whereas the surface albedo impact is observed throughout the year. Because of this difference, the estimated impact in the Amazonian annual radiative budget due to surface albedo-change is approximately 6 times higher than the impact due to aerosol emissions. The influence of atmospheric water vapour content in the radiative budget was also studied

using AERONET column water vapour. It was observed that column water vapour is in average smaller by about 0.35 cm over deforested areas compared to forested areas. Our results indicate that this drying impact contributes to an increase in the shortwave radiative effect that varies from 0.4 W m^{-2} to 1.2 W m^{-2}, depending on the column water vapour content before deforestation.

The large radiative forcing values presented in this study point out that deforestation has strong implications in convection, cloud development and photosynthesis rate over the Amazon region.

1 Introduction

Amazonia is one of the regions that is experiencing fast environmental change with important climatic implications, and has been studied through the LBA (The Large Scale Biosphere-Atmosphere Experiment in Amazonia) experiment (Davidson et al., 2012). It is well established that tropical rainforests are critically important in the global hydrological cycle and in the global carbon budget (Davidson and Artaxo, 2004). Natural aerosols from Amazonia have been recently reviewed and indicate that in the wet season, Amazonia presents very pristine aerosol concentrations, typical of continental pre-industrial atmosphere (Martin, 2010a, b; Pöschl et al., 2010). Tropical emissions from biomass burning from deforestation and agricultural practices play a major role in controlling atmospheric composition especially in the Southern Hemisphere (Bowman et al., 2009). Smoke from fires after deforestation have a large impact in convection, cloud formation and affects the precipitation regime (Andreae et al., 2004; Koren et al., 2008). Aerosols from biomass burning have also been associated with precipitation pattern changes such as the delay in the beginning of the Amazon Basin's dry season (Butt et al., 2011; Bevan et al., 2009). The accumulated deforested area over the Amazon Basin until 2011, was approximately 741 365 km^2 (INPE – PRODES, 2012), or around 18 % of the original forest area. The large area that was deforested changes the radiative budget due to surface albedo changes. However, the rate of deforestation

has significantly decreased since 2004 as reported by INPE – PRODES, 2012. In that year, 2004, 27 000 km^2 were deforested, while only 6200 km^2 were deforested in 2011 (Fig. 1).

Biomass burning aerosols can affect the radiative budget directly by scattering and absorbing solar radiation and indirectly by acting as cloud condensation nuclei and changing cloud properties, such as cloud albedo, lifetime and precipitation rate (Haywood et al., 2000; Forster et al., 2007). Land use change from forest to crops or pasture also changes the evapotranspiration rate with consequences on the water vapour column (Betts et al., 2010).

Long term aerosol monitoring in Amazonia through AERONET sunphotometers (Holben et al., 1998) shows very high aerosol optical depth (AOD) at point locations distributed widely over the region. Figure 2 shows the AOD time series for 3 sites located in the Amazon Basin. This graph illustrates the high seasonality in the aerosol loading as well as large spatial heterogeneity. Comparing the temporal pattern of deforestation and the AOD measurements, it is easy to observe that although deforestation rate have continuously decreased from 2004 on, AOD variability does not follow the same pattern. This indicates that there was a shift in biomass burning activities, initially from deforestation fires and latter associated with pasture and agricultural fires. The high atmospheric loading of biomass burning particles also have important effects on the ratio of diffuse to direct radiation (Yamasoe et al., 2006) that leads to significant increase in net ecosystem exchange (NEE), that can be enhanced by 30–40 % at several observation sites in Amazonia (Oliveira et al., 2007). This increase happens when AOD increase from the background value of 0.1 at 550 nm to about 1.0. For further increase in AOD, the attenuation of the total solar flux starts to dominate and NEE goes to zero.

The assessment of the impacts of biomass burning aerosols in the radiation budget was previously performed in several studies using remote sensing (e.g. Patadia et al., 2008; Christopher et al., 2000). Some of these studies analyzed Clouds and the Earth's Radiant Energy System (CERES) and Moderate Resolution Imaging

SpectroRadiometer (MODIS) or Multi-Angle Spectroradiometer (MISR) AOD retrievals in order to study the effects of aerosols on the radiative budget.

The main goal of this work was to assess the temporal and spatial distributions of the direct aerosol radiative forcing at the top of the atmosphere (TOA) over the Amazon Basin and Brazilian cerrado areas during the biomass burning season. This work was based on ten years of CERES and MODIS simultaneous retrievals. The biomass burning aerosol forcing over areas with different surface reflectivity properties (forest and cerrado) was analysed. This work also aimed to assess the radiative forcing due to changes in surface albedo. This is an important and frequently overlooked issue in tropical regions. The shortwave radiative impact of the reduction in water vapour column over deforested areas in the radiative budget was also investigated. Due to the large land use change in the tropics and high atmospheric aerosol loading from biomass burning, it is clear that biomass burning emissions, changes in surface albedo and changes in water vapour column have profound influences on the radiative balance in Amazonia.

2 Remote sensing methodology

CERES shortwave fluxes and MODIS aerosol optical depth retrievals over the Amazon Basin obtained during the months of August and September (peak of the biomass burning season) from 2000 up to 2009 were analyzed. The CERES sensor aboard the Terra satellite provides radiance measurements in the shortwave (0.3–5.0 µm), infrared window (8.0–12.0 µm) and total (0.3–200 µm) broadband channels (Wielicki et al., 1996). As part of the CERES production line radiances are converted to fluxes using angular dependence models (Loeb et al., 2005, 2007). The main dataset used was the CERES Single Scanner Footprint (SSF) product. In addition to the shortwave and longwave fluxes, this product also contains MODIS (MOD04) aerosol and cloud properties (Remer et al., 2005) and meteorological information computed by the Global Modelling and Assimilation Office (GMAO)'s Goddard Earth Observing System (GEOS)

Data Assimilation System (DAS). MODIS aerosol data, originally available at 10 km of spatial resolution, was translated onto CERES 20 km resolution by using point spread functions (Smith et al., 1994). The most recently available CERES Terra SSF Editions 2B/2F/2G – Rev1 were used in the analyses.

Simultaneous remote sensing retrievals have been used before for the evaluation of the aerosol radiative forcing over oceans and deserts (Zhang et al., 2003, 2005). Patadia et al. 2008 used coincident CERES flux retrievals and MISR AOD retrievals to evaluate the direct radiative forcing of aerosols over the Amazon Basin. Regardless of MISR multiangle feature, we opted to use MODIS's AOD due to its larger swath width and consequently higher spatial coverage. The methodology used in this work is summarized in Fig. 3 and will be detailed in the following sections.

2.1 Cloud-free pixel selection

One of the goals of this study is the assessment of the direct aerosol effect, therefore only cloud-free satellite retrievals were used in the calculations. For that reason we used data from CERES and MODIS sensors, with morning overpasses (approximately at 10:30 a.m., local time), when the region is usually less cloudy than in the afternoon overpasses. Furthermore, a pixel selection strategy was put in place based on MODIS cloud fraction and surface reflectance retrievals, and geometrical constraints on illumination and viewing angles. Pixels with 1 km resolution MODIS cloud fraction above 0.5 % were removed. Pixels with clear area in the MODIS 250 m resolution lower than 99.9 % were also removed. In order to limit distortions we removed from our analysis pixels which presented view and solar zenith angles greater than 60° (similarly as in Patadia et al., 2008). CERES' shortwave broadband channel (0.3–5.0 µm) includes the water vapour absorption band, and thus pixels containing inland water bodies need to be removed. The assessment and removal of inland water pixels was performed using the MODIS 8-day 500 m resolution average surface reflectance product (Vermote et al., 1999). CERES pixels that presented surface reflectance lower than 0.15 in the MODIS 1.2 µm channel in more than 15 % of their footprint were removed.

2.2 Grid cell classification according to surface type

The direct radiative forcing of biomass burning aerosols over the different surface types that compose the studied region (forest and cerrado) was investigated. The area under study was limited between the coordinates 3° N–20° S, 45° W–65°,W and 3° N–11° S, 65° W–74° W. After the pixel selection step the area was divided in 0.5° × 0.5° (latitude/longitude) grid cells. The cell size was chosen so as to maximize the amount of valid pixels in each cell and to minimize surface heterogeneity. The estimated broadband surface albedo from CERES was used to classify each cell according to the surface type. This parameter is derived by weighting the percent coverage of each International Geosphere-Biosphere Programme (IGBP) surface type (Loveland et al., 1997) within the CERES' field of view by the corresponding broadband surface albedo. The albedo look-up tables are based on field observations. In this work, if the average cell broadband albedo was less than 0.140 it was classified as forest; if the average broadband albedo was greater than 0.155 the cell was classified as cerrado; otherwise (albedo values between 0.140 and 0.155) the cell was classified as a transition region. These thresholds were defined based on the frequency distribution of the surface albedo over forest and cerrado covered areas. The analysis of the direct radiative forcing and forcing efficiency of biomass burning aerosols over forest and cerrado areas is presented in Sect. 3.2.

2.3 Methodology for the instantaneous aerosol direct radiative forcing calculation

The mean shortwave aerosol radiative forcing at the TOA (SWARF) during the biomass burning season was defined as the difference between the mean radiative flux at the TOA in clean conditions (F_{cl}) and in polluted conditions (F_{pol}) observed in the studied period. In order to obtain F_{cl} the instantaneous shortwave radiative flux at the TOA, observed during the satellite timepass, was plotted against the AOD for each 0.5° × 0.5° cell. For each cell, linear fits were adjusted to the data points observed for

the biomass burning season of each year. To ensure linearity in the fittings, the maximum AOD for each linear regression was limited to 2. The intercept of each linear fit provides the value of the shortwave radiation flux at the TOA at the limit when AOD = 0 for each grid cell. This value was assumed to be the flux at the TOA for clean conditions and used in the evaluation of the shortwave aerosol radiative forcing. Fig. 4 illustrates two examples in which this procedure was used to evaluate the flux for clean conditions over forest and cerrado covered areas. Notice that by following this procedure the definition of the direct radiative forcing of aerosols used in this work considers the total effect of aerosols including the small contribution of background aerosols in Amazonia (of approximately AOD = 0.1 at 550 nm). To estimate the uncertainty of $SWARF_{24h}$ the uncertainty of the points in each 0.5° × 0.5° cell was estimated by setting the reduced chi-squared equal to 1. The covariance between the flux for clean conditions (F_{cl}) and the mean polluted flux observed during the studied period was also considered in this calculation. To ensure good statistics of data in each cell, cases with less than 10 points or with linear correlation lower than 0.2 were excluded from the analysis. The instantaneous SWARF was expanded to 24 h average ($SWARF_{24h}$) according to the procedure explained in Sect. 2.5.

2.4 Methodology for the assessment of the surface albedo change radiative forcing

In the Amazon Basin, deforestation is expected to generate a negative radiative forcing due to the increase in the surface albedo of the deforested area. Unlike the aerosol direct radiative forcing, which presents marked seasonality, deforestation likely triggers a permanent change in the radiative budget over the impacted area. In this work we quantified the shortwave land-use change radiative forcing (LURF) over deforested areas in Rondônia, a region that has been deforested since the 70's. Deforested and forested regions were selected and classified according to the visual inspection of MODIS red, green and blue (RGB) composite images. Their locations are listed in Table 1 and illustrated in Fig. 5. Deforested areas were denominated D1 and D2 and the

forested area was denominated F2. The chosen regions have approximately the same geometrical area and are located between the same latitude ranges. They present similar characteristics concerning mean water vapour content and mean solar zenith angle during the studied period.

The selected deforested and forested areas were divided into $0.5^{\circ} \times 0.5^{\circ}$ cells. For each cell the instantaneous flux at the TOA for clean conditions (AOD = 0) was evaluated from the intercept of the linear fit of CERES flux at the TOA by AOD. All valid data during the biomass burning seasons from 2000 to 2009 were used to evaluate the flux for clean conditions. T-Student's factor correction was applied to the uncertainty of the flux at the TOA of deforested and forested areas, due to the small number of cells in each region (only 8 valid cells). In analogy to the instantaneous SWARF, the instantaneous LURF was also expanded to 24 h average as will be shown in the next section.

2.5 Evaluation of the mean daily aerosol and surface albedo change radiative forcings

The discrete-ordinate radiative transfer (DISORT) code SBDART (Santa Barbara DISORT Atmospheric Radiative Transfer) (Richiazzi et al., 1998) was used for the assessment of both the mean daily direct radiative forcing of aerosols ($SWARF_{24h}$), and the mean daily surface albedo change radiative forcing due to deforestation ($LURF_{24h}$). The methodology used to expand the instantaneous forcing values to 24 h averaged values will be detailed in the following subsections.

2.5.1 Surface models

The use of a radiative transfer code to evaluate the ascending flux at the TOA requires care in the choice of the simulated surface, due to the large contribution of the surface albedo for the outgoing shortwave radiative flux. In this work MODIS BRDF/Albedo

Model product was used in the assessment of the spectral dependence of the albedo for forest, cerrado and deforested areas.

The solar zenith angle dependence of the directional hemispherical reflectance (black-sky albedo) and of the bihemispherical reflectance (white-sky albedo) can be parameterized by polynomial functions as described by Lucht et al. (2000). The MODIS BRDF/Albedo Model product (Schaaf et al., 2002) provides the weighting parameters for the anisotropy models used to derive the black-sky and white-sky albedos at seven spectral bands (0.470, 0.555, 0.648, 0.858, 1.24, 1.64, 2.13 µm). These are calculated from a combination of Terra and Aqua retrievals every 16-day overpass at a resolution of 1 km.

Four areas were selected to build the surface models used in the radiative transfer code to represent cerrado (savannah-like vegetation, C) and forest covered areas (F1), deforested (D1 and D2) and forested (F2) regions (Table 1). For each area the mean white-sky and black-sky albedos as a function of the solar zenith angle were obtained at 7 wavelengths, using MODIS BRDF/Albedo Model (MCD43B1) retrievals. The diffuse fraction of radiation reaching the surface varies according to the illumination geometry and aerosol loading. The actual albedo (blue-sky albedo) is a linear combination of the black-sky and white-sky albedos (Lucht et al., 2000; Schaaf et al., 2002). It was evaluated by using a look-up table that associates the AOD and solar zenith angle to the diffuse fraction for each wavelength. The spectral dependence of the albedo was obtained by the linear interpolation of the blue-sky albedo in those seven wavelengths, for each 0.1 AOD step and 1° solar zenith angle step.

2.5.2 Aerosol model

AERONET is a federation of ground-based remote sensing aerosol network of well-calibrated Sun/sky radiometers (Holben et al., 1998). AERONET inversion algorithm (Dubovik et al., 2000) provides mean aerosol properties in the atmospheric column derived from the direct and diffuse radiation measured by AERONET sun/sky radiometers. In this work the aerosol model used as an input in the radiative transfer code

was obtained from Level 2.0 (cloud-screened and quality assured) inversion data retrieved in all AERONET sites within the selected region from 2000–2009, during the biomass-burning season (August to September). The mean values observed during the dry season for the aerosol properties (single scattering albedo (ω_0), asymmetry parameter (g) and extinction efficiency factor (Q_{ext})) in 4 wavelengths (440, 670, 870 and 1064 nm) were used in the SBDART simulations (Table 2). The mean Angström exponent between the wavelengths 0.44 and 0.87 µm observed during the period was considered in the simulations (1.647 ± 0.002). These values show good agreement with other authors' previous estimates for smoke aerosol properties over the Amazonia (e.g. Dubovik et al., 2002; Procopio et al., 2003; Schafer et al., 2008).

2.5.3 SBDART simulation

The surface and aerosol models detailed in Sects. 2.5.1 and 2.5.2 were used in SBDART to evaluate the mean daily aerosol radiative forcing ($SWARF_{24h}$) during the Amazonia's biomass burning season. The wavelength range selected for the simulations varied from 0.3 to 5.0 µm, corresponding to the CERES shortwave channel. The mean day of the period (day 243) and the mean column water vapour content for forest regions (3.3 cm) and cerrado regions (2.1 cm) were considered in the simulations, which were run in 0.1 AOD steps and 1° solar zenith angle steps. The solar zenith angle dependence with time for day 243 was obtained for every 2° of latitude. Those functions were interpolated by 1000 points cubic splines. This procedure leads to two look-up tables: the first one relates the 24 h average aerosol radiative forcings to latitude, aerosol optical depth and surface type ($SWARF^{SBDART}_{24h}$ (τ, Lat, Surf)) and the second, relates the instantaneous radiative forcing to solar zenith angle, AOD and surface type ($SWARF^{SBDART}_{Inst}$ (θ_0, τ, Surf)).

For each $0.5^\circ \times 0.5^\circ$ cell, the $SWARF_{24h}$ was calculated by weighting the instantaneous SWARF obtained from CERES-SSF data by the ratio of the daily SWARF over the instantaneous SWARF obtained from SBDART simulations (Remer and Kaufman,

2006). The surface type, mean latitude, mean aerosol optical depth and mean solar zenith angle in each cell were considered for the weighting.

$$SWARF_{24h}(\tau, Lat, Surf) = SWARF^{CERES}_{Inst}(\theta_0, \tau, Surf)\,\frac{SWARF^{SBDART}_{24h}(\tau, Lat, Surf)}{SWARF^{SBDART}_{Inst}(\theta_0, \tau, Surf)} \quad (1)$$

The weighting factor for the $SWARF_{24h}$ for transition areas were estimated by averaging the weighting factors calculated for forest and cerrado regions.

For the evaluation of the surface albedo change radiative forcing a procedure similar to the one above was used, considering the corresponding surface models and AOD = 0. The mean latitude of the deforested and forested areas (11.00° S) and the mean column water vapour amount (3.0 cm) observed for the studied period were used.

3 Results and discussions

3.1 Temporal and spatial distribution of the direct radiative forcing

The mean direct radiative forcing of biomass burning aerosols and its spatial distribution were assessed over the Amazon Basin using the methodology explained in Sect. 2. Table 3 shows the results obtained for the mean and standard deviation of the AOD, instantaneous SWARF and $SWARF_{24h}$ for the studied region during the biomass burning season from 2000 to 2009.

Notice that the standard deviation values shown in Table 3 represent the spatial variability of each variable and not its uncertainty. This variability is due to differences in source locations and in aerosol transport and concentration. Individually for each year, the uncertainty in the mean value of the SWARF is much smaller, approximately 10^{-1} W m^{-2}. The year 2004 was not considered in the analysis due to the lack of valid data in that year. This lack of data was caused by the stringent cloud-screening criteria used in the selection of valid pixels. The remaining non-cloudy pixels were located at a small area that was not representative of the entire studied area.

The results shown in Table 3 indicate that the aerosol radiative forcing at the TOA presents large spatial and temporal variations during the biomass burning season. The smaller mean SWARF values observed for the years 2008 and 2009 are due to the decrease in biomass burning emissions during those years.

The analysis of the spatial distribution of the aerosol radiative forcing allows us to assess the most and less impacted areas due to the presence of aerosol. Two examples of the spatial distribution of the AOD, $SWARF_{24h}$ and its estimated uncertainty during the months of August and September of 2005 and 2008 are given in Fig. 6.

Figure 6 shows the decrease in the absolute value of the radiative forcing at TOA in all Amazon regions from 2005 to 2008, consistent with the reduction in the average AOD value observed in the period (Table 3). For regions where the aerosol loading was very high (AOD > 1), $SWARF_{24h}$ values as negative as $-20\,W\,m^{-2}$ may be observed. Areas located in Eastern Amazon show a smaller radiative forcing due to the smaller concentration of aerosols over the region and also to the higher surface reflectance of those areas. In 2005 there is a strong correlation between the radiative forcing and AOD. In 2008 such correlation is still observed, but it is less intense than the one presented in 2005. This difference in the correlation intensities is due to the smaller average AOD value presented in 2008 when compared to 2005. In addition to the aerosol loading other parameters such as the surface albedo, water vapour amount and solar illumination also play a role in the final radiative forcing value. These influences will be explored in the next sections.

3.2 Surface type influence in the direct aerosol radiative forcing

The aerosol impact over different surface types was studied using the grid cell classification methodology explained in Sect. 2.2. In order to evaluate forest and cerrado forcing efficiencies at 550 nm the pixels were grouped according to surface type and a linear fit of the radiative flux at the TOA by AOD was derived for each surface type, for each year. The aerosol forcing efficiencies were obtained from the slope of the linear regressions for each surface type. For this procedure it was assumed that the surface

and aerosol optical properties remained the same during the months of August and September of each year. These assumptions may introduce other uncertainty sources besides the instrumental error of the sensor. For that reason, the uncertainties in the intercept and the slope of the regression were recalculated by setting the reduced chi-squared equal to 1. The values obtained for the instantaneous aerosol forcing efficiency, and the ascending TOA flux for clean conditions for forest and cerrado, during the biomass burning seasons of the years 2000 to 2009 are listed in Table 4.

The difference of approximately $13\,W\,m^{-2}$ between forest and cerrado instantaneous fluxes at the TOA for clean conditions is mainly due to surface albedo differences for these regions. Regions covered by forest absorb more solar radiation and therefore the upward flux at the TOA over cerrado regions is larger than over forest regions for a given illumination and viewing geometry. The values of the mean daily TOA forcing efficiency of aerosols over forest and cerrado regions are $-15.7 \pm 2.4\,W\,m^{-2}/\tau_{550\,nm}$ and $-9.3 \pm 1.7\,W\,m^{-2}/\tau_{550\,nm}$, respectively. The forcing efficiency results indicate that Amazon regions with lower surface albedo are subject to a more significant radiative forcing (that is, greater in modulus) than regions of brighter soil, considering the same aerosol type. In other words, the impact of biomass burning aerosols is larger over forest than over cerrado. These results point out the necessity of treating forest and cerrado areas as different entities, which will experience different impacts due to the presence of biomass burning aerosols.

The 24 h average aerosol forcing efficiency of the selected region as a whole, representing a significant fraction of the Amazon Basin, is $-13.1 \pm 1.6\,W\,m^{-2}/\tau_{550\,nm}$. This value was estimated by considering the analysed area as composed by 40 % of savannah-like vegetation and 60 % of forest vegetation.

The $SWARF_{24h}$ was also analysed separately for forest and cerrado regions (Table 5). Table 5 shows systematically more negative $SWARF_{24h}$ values for forest regions when compared to cerrado regions. The mean daily radiative forcing of biomass burning aerosols observed during the studied period was $-6.2 \pm 1.9\,W\,m^{-2}$ over forest and $-4.6 \pm 1.6\,W\,m^{-2}$ over cerrado. This is due to a combination of two effects: (i) the

higher aerosol concentration over forest, due to the East-West wind pattern over the region, and (ii) the higher aerosol impact over darker surfaces (higher AOD and higher forcing efficiency over forest regions).

3.3 Evaluation of the surface albedo change radiative forcing over Rondônia

The land-use change radiative forcing (LURF) due to surface albedo change caused by deforestation was assessed over Rondônia following the methodology explained in Sect. 2.4. The selected deforested area (Table 1 and Fig. 5, area D1 + D2) covers approximately 20 000 km^2.

The values obtained for the LURF over Rondônia for the dry season from 2000 to 2009 were $-23.7 \pm 2.9\,W\,m^{-2}$ for the instantaneous shortwave forcing and $-7.1 \pm 0.9\,W\,m^{-2}$ for the mean daily forcing. These results show that the surface albedo change radiative forcing due to deforestation is comparable to the mean direct radiative forcing of aerosols during the biomass burning season. Nevertheless it is important to consider that emission of biomass burning aerosols is seasonal, while the impact of surface albedo change is observed during the whole year. The yearly average of the surface albedo change radiative forcing over the selected deforested area is $-7.3 \pm 0.9\,W\,m^{-2}$. This last value was evaluated considering daily changes in the ascending solar irradiation at the TOA over the studied area. An assessment of the yearly average of the SWARF over cloud-free sky leads to a value that varies from $-0.9 \pm 0.3\,W\,m^{-2}$, to $-1.4 \pm 0.4\,W\,m^{-2}$ considering that the biomass burning season lasts approximately 2 to 3 months. In temperate latitudes there is a large seasonal variation in the surface albedo, but near the tropics the seasonal variation in surface albedo is expected to be relatively low. In order to compare the impacts of the aerosol and the land-use change radiative effects over cloud-free sky, in this assessment it was assumed that the surface albedo does not change significantly during the year. Therefore the two-month period calculation was used to extrapolate for the annual mean of the surface albedo change radiative forcing. This analysis indicated that, on a yearly basis,

the surface albedo change radiative impact can be more than 6 times higher than the aerosol impact over the Amazon Basin for cloud-free conditions.

Deforested regions tend to be drier than forested regions, due to the smaller evapotranspiration over the area after the removal of forests. The impact of deforestation in the atmospheric water vapour content was studied over deforested (Ji Paraná – Abracos Hill) and forested (Reserva Biológica Jaru) AERONET stations. The selected sites are approximately 86 km apart. They are relatively close to each other and it is assumed they are subject to similar meteorological conditions. The mean difference in the water vapour amount retrieved by AERONET sunphotometers over the two stations from July to October 2002 was approximately 0.35 cm (Fig. 7). The behaviour of the shortwave surface albedo change radiative effect at the TOA with column water vapour content and latitude was studied. The spectral surface albedo dependence for forested and deforested regions obtained according to Sect. 2.5.1, were used as surface models in the SBDART radiative transfer code. The spectral range selected for the simulations was chosen to match CERES shortwave channel spectral range (0.3 to 5.0 µm). In the simulations, SBDART tropical atmospheric profile was used, and the total column water vapour amount was varied from 1.5 to 5.0 cm in 0.5 cm steps. Those were the typical column water vapour values observed for the studied region during the biomass burning season. Two different situations were considered for the study of the influence of water vapour in the $LURF_{24h}$: (i) considering that the water vapour amount is conserved after deforestation and (ii) considering that the deforested region is 0.35 cm drier after deforestation. Figure 8 shows that the surface albedo change impact is higher for situations when the amount of radiation reaching the surface is larger, that is, closer to the Equator and for lower atmospheric water vapour contents, due to gaseous absorption of infrared radiation. The surface albedo radiative forcing due to deforestation is approximately $1.2\,W\,m^{-2}$ more negative for sites located at latitude 0° than for sites located at latitude 20° S, considering the same column water vapour content for both regions.

Taking into account the drying effect, the amount of radiation reaching the surface after deforestation will be even larger due to the smaller infrared radiation absorption by water vapour. This will lead to even more pronounced radiative effects at the top of the atmosphere. Figure 8 (dashed lines) indicates that this drying impact contributes to an increase in the radiative effect that varies from 0.4 W m^{-2} to 1.2 W m^{-2}, depending on the column water vapour content before deforestation. Those results highlight the importance of considering water vapour and solar zenith angle variations when evaluating radiative effects.

4 Discussions

In this section we will discuss the main results presented in this work and compare them with other evaluations available in literature. The comparison between aerosol forcing efficiency results requires care, since there is not a uniform methodology in the scientific community on how to obtain this quantity. Li et al. (2000), Christopher et al. (2002), and Procopio et al. (2004) calculated the forcing efficiency at wavelengths of 640 nm, 670 nm and 500 nm, respectively. In order to understand the differences associated with the wavelength dependence of the forcing efficiency and to standardize it, the forcing efficiency at 550 nm was estimated, assuming a value of 1.647 for the Angström exponent, according to AERONET retrievals during the dry season. This normalization to 550 nm increases by 17 % the forcing efficiency value calculated at 500 nm, and decreases by 28 % the forcing efficiency calculated at 670 nm. This analysis illustrates the large spectral dependence of the forcing efficiency of biomass burning aerosols.

Several authors have derived only the instantaneous direct aerosol radiative forcing and/or its forcing efficiency over the Amazon Basin (e.g. Christopher et al., 2000, 2002; Li et al., 2000; Patadia et al., 2008). These assessments were made using retrievals from different instruments onboard satellites (e.g. GOES-8, TRMM, Terra) or using in situ aerosol optical properties measurements into radiative transfer models

and assuming a given solar geometry. The problem in considering a particular illumination geometry is that the aerosol radiative forcing and forcing efficiency strongly depend on solar zenith angle. Furthermore instantaneous assessments only help us understand the aerosol impact over a given area qualitatively. For those reasons we have chosen not to compare instantaneous radiative forcing and forcing efficiencies results. The comparison between the 24 h average results reported in this work and in previous studies is shown in Table 6.

Table 6 shows that the mean daily aerosol radiative forcing results over the Amazon Basin are compatible with other authors work. Patadia et al. (2008) assessment of the direct aerosol radiative forcing was made from 2000 to 2005 when the aerosol loading was higher than during the period considered in this work. When compared to their work, the impact of the aerosols assessed by our work is around 2 W m^{-2} smaller (less negative). This result is consistent with this decrease in the average aerosol optical depth.

The mean daily aerosol forcing efficiency values obtained for forest and cerrado regions are compatible with results reported by Ross et al. (1998). The high uncertainty observed in their results is due to the observed variability in aerosol scattering and absorption coefficients.

As pointed out in Sect. 3.3 although the mean aerosol and surface albedo change radiative forcings magnitudes are similar during the biomass burning season (Table 6), the impact of biomass burning aerosols is seasonal while the impact of land-use change may be observed throughout the year. This difference indicates that the yearly local impact of surface albedo change in the radiative balance is more than 6 times higher than direct impact of aerosols.

5 Summary and conclusions

This work focused on understanding the impact of aerosol emissions following biomass burning from deforestation on the radiation balance over the Amazon Basin using

remote sensing. CERES and MODIS retrievals were used to assess the temporal and spatial distributions of the direct radiative forcing of biomass burning aerosols over the Amazon Basin and the surface albedo change radiative forcing over Rondônia, both caused by deforestation. AERONET and MODIS BRDF data were used to build aerosol and surface models, respectively. These models were used in the radiative transfer code SBDART to convert instantaneous radiative forcing values into mean daily values.

The average daily direct radiative forcing of aerosols at the TOA was $-5.6 \pm 1.7\,\mathrm{W\,m^{-2}}$ from 2000 to 2009 during the biomass burning season (August and September). The spatial distribution analysis of the direct radiative forcing shows large geographical variability with significant impacts of aerosols over Central and South-western Amazon. Daily averaged TOA radiative forcing values as high as $-20\,\mathrm{W\,m^{-2}}$ were observed for AOD higher than 1.0 at 550 nm.

We also observed that land surface properties strongly impact the direct radiative forcing of aerosols. The assessment of the direct radiative forcing over different surface types indicates that the impact of biomass burning aerosols in the energy budget is higher over forest than over cerrado (savannah-like) covered regions. The mean daily direct radiative forcing was 35 % higher over forest than over cerrado during the studied period. Two factors contribute to this difference: (i) the typical East-to-West wind pattern, which in average transports aerosols to large forest-covered areas, and (ii) the stronger aerosol forcing efficiency of aerosols over darker regions. The mean daily forcing efficiencies of forest and cerrado (savannah-like) vegetation were $-15.7 \pm 2.4\,\mathrm{W\,m^{-2}}/\tau_{550\,\mathrm{nm}}$ and $-9.3 \pm 1.7\,\mathrm{W\,m^{-2}}/\tau_{550\,\mathrm{nm}}$, respectively.

In addition to biomass burning aerosol emissions, deforestation also impacts the radiative balance by changing surface albedo of the deforested area. This modification may alter convection processes, cloud formation and the precipitation regime over the area. A value of $-7.3 \pm 0.9\,\mathrm{W\,m^{-2}}$ was estimated for the mean annual albedo-change radiative forcing over Rondônia. The mean annual direct radiative forcing of biomass burning aerosols was estimated at $-0.9 \pm 0.3\,\mathrm{W\,m^{-2}}$ over cloud-free skies, considering

that the biomass burning season lasts approximately two months. Those results reveal the large impact of land use change from deforestation over Amazonia's energy budget. To our knowledge, this is the first time such an assessment was made over the Amazon combining the changes in surface albedo, water vapour and aerosols.

Deforestation also contributes to the decrease of the water vapour amount over the deforested region. The impact of deforestation in humidity was assessed using AERONET column water vapour measurements over deforested and forested areas nearby. The analysed deforested area was 0.35 cm drier than the forested area. This decrease in the atmospheric water vapour content further enhances the effect of deforestation in the radiative balance. The results presented herein, point out the necessity to further investigate the combined impacts of water vapour and surface property changes in the Amazon Basin and in the global radiative balance.

Acknowledgements. The authors would like to thank Lorraine Remer and José Vanderlei Martins for the helpful suggestions and for the revision of the manuscript of this paper. We also thank FAPESP and CNPq for the financial support. CERES-SSF data were obtained from the Atmospheric Science Data Center at the NASA Langley Research Center. We thank INPA (The Brazilian National Institute for Research in Amazonia) for LBA support.

References

Andreae, M. O., Rosenfeld, D., Artaxo, P., Costa, A. A., Frank, G. P., Longo, K. M., and Silva-Dias, M. A. F.: Smoking rain clouds over the Amazon, Science, 303, 1337–1342, 2004.

Betts, A. K. and Silva Dias, M. A. F.: Progress in understanding land-surface-atmosphere coupling from LBA research, J. Adv. Model. Earth Syst., 2, ,6, 20 pp., doi:10.3894/JAMES.2010.2.6, 2010.

Bevan, S. L., North, P. R. J., Grey, W. M. F., Los, S. O., and Plummer, S. E.: Impact of atmospheric aerosol from biomass burning on Amazon dry-season drought, J. Geophys. Res., 114, D09204, doi:10.1029/2008JD011112, 2009.

Bowman, D. M. J. S., Balch, J. K., Artaxo, P., Bond, W. J., Carlson, J. M., Cochrane, M. A., D'Antonio, C. M., Defries, R. S., Doyle, J. C., Harrison, S. P., Johnston, F. H., Keeley, J. E.,

Krawchuk, M. A., Kull, C. A., Marston, J. B., Moritz, M. A., Prentice, I. C., Roos, C. I., Scott, A. C., Swetnam, T. W., Van der Werf, G. R., and Pyne, S. J: Fire in the Earth System, Science, 324, 481–484, doi:10.1126/science.1163886, 2009.

Butt, N., de Oliveira, P. A., and Costa, M. H.: Evidence that deforestation affects the onset of the rainy season in Rondonia, Brazil, J. Geophys. Res., 116, 2–9, doi:10.1029/2010JD015174, 2011.

Christopher, S. A., Li, X., Welch, R. M., Reid, J. S., Hobbs, P. V., Eck, T. F., and Holben, B.: Estimation of surface and top-of-atmosphere shortwave irradiance in biomass-burning regions during SCAR-B, J. Appl. Meteorol., 39, 1742–1753, 2000.

Christopher, S. A. and Zhang, J.: Daytime Variation of Shortwave Direct Radiative Forcing of Biomass Burning Aerosols from GOES-8 Imager, J. Atmos. Sci., 59, 681–691, doi:10.1175/1520-0469(2002)059<0681:DVOSDR>2.0.CO;2, 2002.

Davidson, E. A. and Artaxo, P.: Globally significant changes in biological processes of the Amazon Basin: Results of the Large-scale Biosphere-Atmosphere Experiment, Glob. Change Biol., 10, 519–529, doi:10.1111/j.1529-8817.2003.00779.x, 2004.

Davidson, E. A., Araújo, A. C., Artaxo, P., Balch, J. K., Brown, I. F., Bustamante, M. M. C., Coe, M. T., DeFries, R. S., Keller, M., Longo, M., Munger, W., Schroeder, W., Soarez-Filho, B. S., Souza, C. M., and Wofsy, S. C.: The Amazon Basin in Transition, Nature, 481, 321–328, doi:10.1038/nature10717, 2012.

Dubovik, O. and King, M. D.: A flexible inversion algorithm for retrieval of aerosol optical properties from Sun and sky radiance measurements, J. Geophys. Res., 105, 20673–20696, doi:10.1029/2000JD900282, 2000.

Dubovik, O., Holben, B., Eck, T., Smirnov, A., Kaufman, Y., King, M., Tanré, D., and Slutsker, I.: Variability of absorption and optical properties of key aerosol types observed in worldwide locations, J. Atmos. Sci., 59, 590–608, 2002.

Forster, P., Ramaswamy, V., Artaxo, P., Berntsen, T., Betts, R. A., Fahey, D. W., Haywood, J., Lean, J., Lowe, D. C., Myhre, G., Nganga, J., Prinn, R., Raga, G., Schulz, M., and Van Dorland, R.: Changes in Atmospheric Constituents and Radiative Forcing, Chapter 2 of the Climate Change 2007: The Physical Science Basis, IPCC – Intergovernmental Panel on Climate Change Book, Cambridge University Press, United Kingdom, ISSN 978-0-521-88009-1, 2007.

Haywood, J.: Estimates of the direct and indirect radiative forcing due to tropospheric aerosols: A review, Rev. Geophys., 38, 513–543, doi:10.1029/1999RG000078, 2000.

Holben, B.: AERONET – A Federated Instrument Network and Data Archive for Aerosol Characterization, Rem. Sens. Environ., 66, 1–16, doi:10.1016/S0034-4257(98)00031-5, 1998.

INPE: Instituto Nacional de Pesquisas Espaciais: Projeto Prodes Monitoramento da Floresta Amazônica Brasileira por Satélite, (http://www.obt.inpe.br/prodes), 2012

Koren, I., Martins, J. V., Remer, L. A., and Afargan, H.: Smoke invigoration versus inhibition of clouds over the Amazon, (New York, NY), Science, 321, 946–949, 2008.

Li, X., Christopher, S. A, Chou, J., and Welch, R. M.: Estimation of Shortwave Direct Radiative Forcing of Biomass-Burning Aerosols Using New Angular Models, J. Appl. Meteorol., 39, 2278–2291, doi:110.1175/1520-0450(2001)040<2278:EOSDRF>2.0.CO;2, 2000.

Loeb, N. G., Kato, S., Loukachine, K., and Manalo-Smith, N.: Angular Distribution Models for Top-of-Atmosphere Radiative Flux Estimation from the Clouds and the Earth's Radiant Energy System Instrument on the Terra Satellite, Part I, Methodology, J. Atmos. Ocean. Tech., 22, 338–351, doi:10.1175/JTECH1712.1, 2005.

Loeb, N. G., Kato, S., Loukachine, K., Manalo-Smith, N., and Doelling, D. R.: Angular Distribution Models for Top-of-Atmosphere Radiative Flux Estimation from the Clouds and the Earth's Radiant Energy System Instrument on the Terra Satellite, Part II, Validation, J. Atmos. Ocean. Tech., 24, 564–584, doi:10.1175/JTECH1983.1, 2007.

Loveland, T. R. and Belward, A. S.: The IGBP-DIS global 1 km land cover data set, DISCover: First results, Int. J. Rem. Sens., 18, 3289–3295, doi:10.1080/014311697217099, 1997.

Lucht, W., Schaaf, C. B., and Strahler, A. H.: An algorithm for the retrieval of albedo from space using semiempirical BRDF models, IEEE T. Geosci. Remote, 38, 977–998, doi:10.1109/36.841980, 2000.

Martin, S. T., Andreae, M. O., Althausen, D., Artaxo, P., Baars, H., Borrmann, S., Chen, Q., Farmer, D. K., Guenther, A., Gunthe, S. S., Jimenez, J. L., Karl, T., Longo, K., Manzi, A., Müller, T., Pauliquevis, T., Petters, M. D., Prenni, A. J., Pöschl, U., Rizzo, L. V., Schneider, J., Smith, J. N., Swietlicki, E., Tota, J., Wang, J., Wiedensohler, A., and Zorn, S. R.: An overview of the Amazonian Aerosol Characterization Experiment 2008 (AMAZE-08), Atmos. Chem. Phys., 10, 11415–11438, doi:10.5194/acp-10-11415-2010, 2010.

Martin, S. T., Andreae, M. O., Artaxo, P., Baumgardner, D., Chen, Q., Goldstein, A. H., Guenther, A. B., Heald, C. L., Mayol-Bracero, O. L., McMurry, P. H., Pauliquevis, T., Pöschl, U., Prather, K. A., Roberts, G. C., Saleska, S. R., Silva Dias, M. A., Spracklen, D. V., Swietlicki, E., and Trebs, I.: Sources and Properties of Amazonian Aerosol Particles, Rev. Geophys., 48, RG2002, doi:10.1029/2008RG000280, 2010.

Oliveira, P. H. F., Artaxo, P., Pires, C. Jr., Lucca, S., Procópio, A., Holben, B., Schafer, J., Cardoso, L. F., Wofsy, S. C., and Rocha, H. R.: The effects of biomass burning aerosols and clouds on the CO_2 flux in Amazonia, Tellus B, 59, 338–349, doi:10.1111/j.1600-0889.2007.00270.x, 2007.

Patadia, F., Gupta, P., Christopher, S. A., and Reid, J. S.: A multisensor satellite-based assessment of biomass burning aerosol radiative impact over Amazonia, J. Geophys. Res., 113, D12214, doi:10.1029/2007JD009486, 2008.

Procopio, A. S., Remer, L. A., Artaxo, P., Kaufman, Y., and Holben, B. N.: Modeled spectral optical properties for smoke aerosols in Amazonia. Geophys. Res. Lett., 30, 2265–2270, doi:10.1029/2003GL018063, 2003.

Procopio, A., Artaxo, P., Kaufman, Y., Remer, L., Schafer, J., and Holben, B.: Multiyear analysis of Amazonian biomass burning smoke radiative forcing of climate, Geophys. Res. Lett., 31, L03108, doi:10.1029/2003GL018646, 2004.

Pöschl, U., Martin, S. T., Sinha, B., Chen, Q., Gunthe, S. S., Huffman, J. A., Borrmann, S., Farmer, D. K., Garland, R. M., Helas, G., Jimenez, J. L., King, S. M., Manzi, A., Mikhailov, E., Pauliquevis, T., Petters, M. D., Prenni, A. J., Roldin, P., Rose, D., Schneider, J., Su, H., Zorn, S. R., Artaxo, P., and Andreae, M. O.: Rainforest aerosols as biogenic nuclei of clouds and precipitation in the Amazon, Science, 329, 1513–1516, doi:10.1126/science.1191056, 2010.

Remer, L. A., Kaufman, Y. J., Tanré, D., Mattoo, S., Chu, D. A., Martins, J. V., Li, R. R., Ichoku, C., Levy, R. C., Kleidman, R. G., Eck, T. F., Vermote, E., and Holben, B. N.: The MODIS aerosol algorithm, products and validation, J. Atmos. Sci., 62, 947–973, 2005.

Remer, L. A. and Kaufman, Y. J.: Aerosol direct radiative effect at the top of the atmosphere over cloud free ocean derived from four years of MODIS data, Atmos. Chem. Phys., 6, 237–253, doi:10.5194/acp-6-237-2006, 2006.

Ricchiazzi, P., Yang, S., Gautier, C., and Sowle, D.: SBDART: A Research and Teaching Software Tool for Plane-Parallel Radiative Transfer in the Earth's Atmosphere, B. Am. Meteorol. Soc., 79, 2101–2114, 1998.

Ross, J., Hobbs, P., and Holben, B.: Radiative characteristics of regional hazes dominated by smoke from biomass burning in brazil: Closure tests and direct radiative forcing, J. Geophys. Res., 103, 31925–31941, 1998.

Schafer, J. S., Eck, T. F., Holben, B. N., Artaxo, P., and Duarte, A.: Characterization of the optical properties of atmospheric aerosols in Amazonia from long term

AERONET monitoring (1993–1995; 1999–2006). J. Geophys. Res.-Atmos., 113, D04204, doi:10.1029/2007JD009319, 2008.

Schaaf, C. B., Gao, F., Strahler, A. H., Lucht, W., Li, X., Tsang, T., Strugnell, N. C., Zhang, X., Jin, Y., Muller, J.-P., Lewis, P., Barnsley, M., Hobson, P., Disney, M., Dunderdale, M. Doll, C., d'Entremont, R. P., Hu, B., Liang, S., Privette, J., and Roy, D.: First operational BRDF, albedo nadir reflectance products from MODIS, Rem. Sens. Environ., 83, 135–148, doi:10.1016/S0034-4257(02)00091-3, 2002.

Smith, G. L.: Effects of time response on the point spread function of a scanning radiometer, Appl. Opt., 33, 7031–7037, 1994.

Vermote, E. F. and Vermeulen, A.: Atmospheric correction algorithm: Spectral reflectance (MOD09), MODIS algorithm technical background document, version 4.0, University of Maryland, Department of Geography, 1999.

Wielicki, B. A., Barkstrom, B. R., Harrison, E. F., Lee, R. B., Smith, G. L., and Cooper, J. E.: Clouds and the Earth's Radiant Energy System (CERES): An Earth observing system experiment, B. Am. Meteorol. Soc., 77, 853–868, 1996.

Yamasoe, M. A., von Randow, C., Manzi, A. O., Schafer, J. S., Eck, T. F., and Holben, B. N.: Effect of smoke and clouds on the transmissivity of photosynthetically active radiation inside the canopy, Atmos. Chem. Phys., 6, 1645–1656, doi:10.5194/acp-6-1645-2006, 2006.

Zhang, J. and Christopher, S. A.: Longwave radiative forcing of Saharan dust aerosols estimated from MODIS, MISR, and CERES observations on Terra, Geophys. Res. Lett., 30, 2188, doi:10.1029/2003GL018479, 2003.

Zhang, J., Christopher, S. A., and Remer, L.: Shortwave aerosol radiative forcing over cloud-free oceans from Terra: 2, Seasonal and global distributions, J. Geophys. Res., 110, D10S24, doi:10.1029/2004JD005009, 2005.

Table 1. Coordinates of forest and cerrado regions and forested and deforested regions used at the SBDART radiative transfer code for obtaining the 24 h SWARF cycle.

Study and area description	Coordinates (Latitute; Longitude)
Surface type study: Forest (F1)	4.5° S–8.0° S; 64.0° W–70.0° W
Surface type study: Cerrado (C)	10.0° S–18.0° S; 46.0° W–48.0° W
Albedo change study: Deforested area 1 (D1)	10.0° S–11.0° S; 62.0° W–63.0° W
Albedo change study: Deforested area 2 (D2)	11.0° S–12.0° S; 61.4° W–62.4° W
Albedo change study: Forested area (F2)	10.0° S–12.0° S; 70.0° W–71.0° W

Table 2. Aerosol optical properties (single scattering albedo (ω_0), asymmetry parameter (g) and extinction efficiency factor (Q_{ext})) obtained from AERONET Lev. 2.0 aerosol inversion product used in the radiative transfer code SBDART.

Wavelength (μm)	0.441	0.673	0.873	1.022
ω_0	0.921 (1)	0.904 (1)	0.885 (1)	0.871 (2)
g	0.680 (1)	0.577 (1)	0.518 (1)	0.491 (1)
Q_{ext}	1.419 (59)	0.703 (29)	0.435 (18)	0.324 (13)

Table 3. Mean aerosol optical depth (AOD), instantaneous shortwave aerosol radiative forcing (SWARF) and daily for the Amazon region SWARF with their respective standard deviation. These calculation were performed for the biomass burning season of the years 2000 to 2009. The standard deviation represents the spatial variability of each parameter.

Year	Valid Cells	AOD (550 nm)	Instantaneous SWARF($W\,m^{-2}$)	Daily SWARF ($W\,m^{-2}$)
2000	1163	0.22 ± 0.12	-12.3 ± 6.6	-7.0 ± 3.4
2001	1492	0.18 ± 0.08	-8.1 ± 4.1	-4.7 ± 2.3
2002	1447	0.31 ± 0.21	-12.8 ± 7.3	-6.5 ± 3.4
2003	1392	0.25 ± 0.14	-12.0 ± 6.5	-6.4 ± 3.0
2004	185	0.11 ± 0.12	-13.4 ± 11.7	-6.7 ± 7.1
2005	1799	0.41 ± 0.24	-15.0 ± 7.9	-7.4 ± 3.3
2006	1654	0.24 ± 0.16	-9.5 ± 5.1	-4.9 ± 2.5
2007	1731	0.41 ± 0.25	-13.9 ± 6.8	-6.9 ± 2.8
2008	1665	0.18 ± 0.12	-8.2 ± 4.2	-4.3 ± 2.6
2009	1405	0.06 ± 0.03	-4.7 ± 2.4	-2.0 ± 2.1
Average*	1528	0.25 ± 0.11	-10.7 ± 3.3	-5.6 ± 1.7

* The year 2004 was excluded from the analysis due to the lack of valid data.

Table 4. Mean TOA shortwave flux for no aerosols and 24 h mean forcing efficiency for forest and cerrado (savannah-like) regions with their respective uncertainties.

	Forest		Cerrado	
Year	TOA Flux for AOD = 0 ($W\,m^{-2}$)	24 h Forcing efficiency ($W\,m^{-2}/\tau_{550\,nm}$)	TOA Flux for AOD = 0 ($W\,m^{-2}$)	24 h Forcing efficiency ($W\,m^{-2}/\tau_{550\,nm}$)
2000	145.76 ± 0.09	-20.20 ± 0.12	159.26 ± 0.13	-9.93 ± 0.23
2001	144.41 ± 0.06	-15.08 ± 0.10	158.20 ± 0.09	-7.79 ± 0.21
2002	145.26 ± 0.07	-14.17 ± 0.06	156.35 ± 0.09	-9.53 ± 0.13
2003	144.39 ± 0.07	-16.18 ± 0.07	158.72 ± 0.10	-8.79 ± 0.19
2004	150.11 ± 0.73	-13.60 ± 0.47	178.48 ± 0.25	-5.23 ± 0.45
2005	148.48 ± 0.07	-13.75 ± 0.05	160.97 ± 0.08	-9.92 ± 0.08
2006	148.18 ± 0.05	-14.89 ± 0.05	159.99 ± 0.10	-10.53 ± 0.13
2007	148.03 ± 0.06	-13.48 ± 0.04	167.51 ± 0.08	-8.48 ± 0.08
2008	150.87 ± 0.06	-14.64 ± 0.08	165.57 ± 0.11	-6.49 ± 0.25
2009	149.96 ± 0.06	-19.28 ± 0.22	155.18 ± 0.12	-12.39 ± 0.67
Average*	147.3 ± 0.8	-15.7 ± 2.4	160.2 ± 1.3	-9.3 ± 1.7

* The year 2004 was excluded from the analysis due to the lack of valid data.

Table 5. Mean aerosol optical depth at 550 nm (AOD) and daily SWARF for forest and cerrado (savannah-like) regions with their respective standard deviation. These calculation were performed for the biomass burning season of the years 2000 to 2009. The standard deviation represents the spatial variability of each parameter.

	Forest		Cerrado	
Year	AOD (550 nm)	SWARF 24 h ($W m^{-2}$)	AOD (550 nm)	SWARF 24 h ($W m^{-2}$)
2000	0.27 ± 0.10	-7.7 ± 3.5	0.16 ± 0.11	-5.9 ± 3.2
2001	0.21 ± 0.07	-5.0 ± 2.4	0.12 ± 0.07	-4.3 ± 2.3
2002	0.38 ± 0.21	-7.3 ± 3.7	0.18 ± 0.15	-5.0 ± 2.6
2003	0.34 ± 0.13	-7.3 ± 3.3	0.14 ± 0.09	-5.3 ± 2.3
2004	–	–	0.10 ± 0.11	-6.0 ± 6.1
2005	0.50 ± 0.20	-7.8 ± 3.4	0.27 ± 0.20	-6.5 ± 2.7
2006	0.27 ± 0.16	-5.2 ± 2.5	0.17 ± 0.13	-4.3 ± 2.4
2007	0.49 ± 0.22	-7.7 ± 2.8	0.29 ± 0.23	-5.7 ± 2.4
2008	0.24 ± 0.11	-4.9 ± 2.3	0.09 ± 0.07	-3.4 ± 2.8
2009	0.07 ± 0.03	-2.4 ± 1.8	0.04 ± 0.03	-1.2 ± 2.2
Average*	0.31 ± 0.14	-6.2 ± 1.9	0.16 ± 0.08	-4.6 ± 1.6

* The year 2004 was excluded from the analysis due to the lack of valid data.

Table 6. Comparison of the aerosol and surface radiative forcing effects with previous studies. These results were calculated during the dry season (August and September) of the period.

Reference	Region	Period	24 h SWARF ($W m^{-2}$)	24 h Forcing efficiency ($W m^{-2}/\tau_{550\,nm}$)	24 h Albedo Change RF ($W m^{-2}$)
This work	Amazon	2000–2009	-5.6 ± 1.7	-13.1 ± 1.6	-7.1 ± 0.9
Patadia et al. (2008)	Amazon	2000–2005	-7.6 ± 1.9	–	–
Procopio et al. (2004)	Amazon	2002	-5.6 ± 0.6[a]	-10.5[b]	–
Procopio et al. (2004)	AF	1993–2002	-8.3 ± 2.0	–	–
Procopio et al. (2004)	AH	1994–2002	-8.4 ± 2.2	–	–
This work	Forest	2000–2009	-6.2 ± 1.9	-15.7 ± 2.4	–
Ross et al. (1998)	Forest	1995	–	-20 ± 7	–
This work	Cerrado	2000–2009	-4.6 ± 1.6	-9.3 ± 1.7	–
Ross et al. (1998)	Cerrado	1995	–	-8 ± 9	–

[a] This value was obtained from the mean $SWARF_{24\,h}$ and its standard deviation for the months August and September of 2002.
[b] The aerosol forcing efficiency was normalized for AOD at 550 nm using an Angstrom exponent value of 1.647.

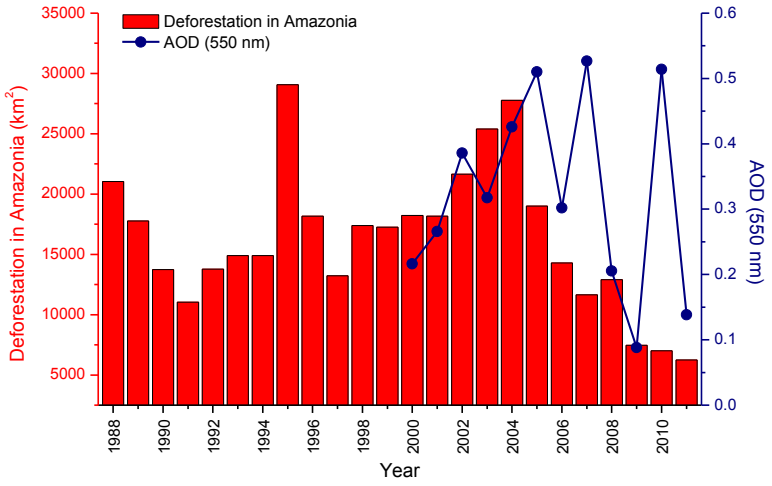

Fig. 1. Deforestation rate in the Amazonia since 1988, showing the high decrease in Amazon deforestation since 2004 (red bars, data extracted from Prodes INPE, 2012). The blue points correspond to the mean AOD at 550 nm retrieved by MODIS during the biomass burning season over the Amazonia. Notice that the aerosol loading does not follow the deforestation pattern. This indicates biomass burning activities aiming the maintenance of pasture and agricultural fields.

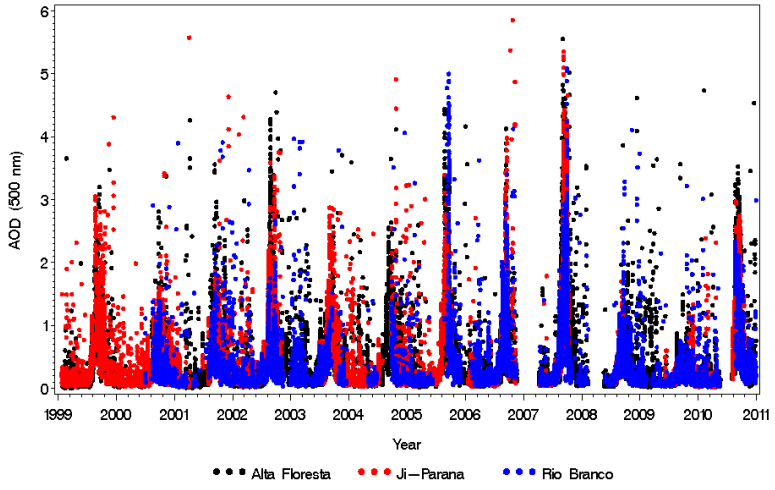

Fig. 2. Time series of aerosol optical depth (AOD) at 500 nm retrieved by AERONET sun-photometer for 3 places in Amazonia: Alta Floresta, Ji-Paraná and Rio Branco. This graph illustrates the high seasonality in the aerosol loading as well as the spatial heterogeneity in the AOD.

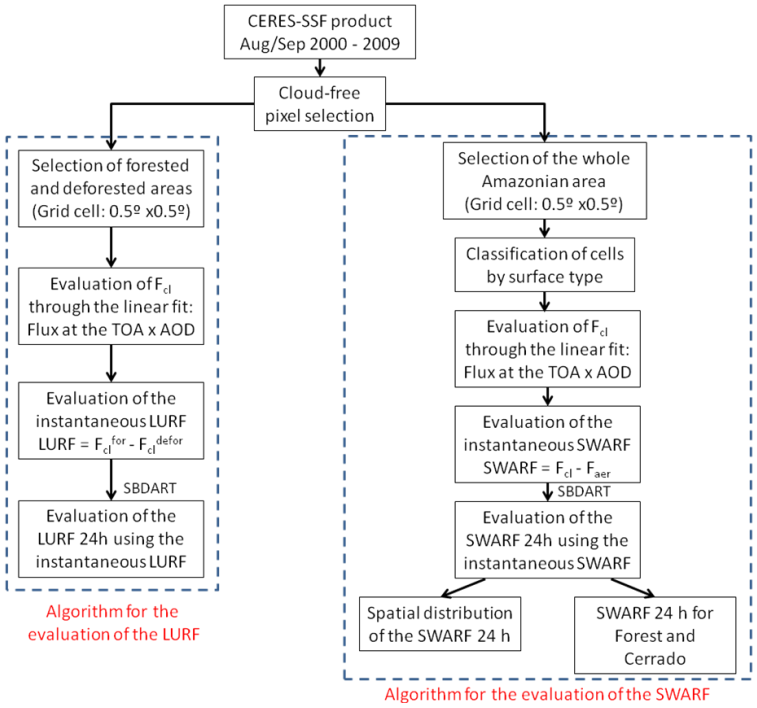

Fig. 3. Simultaneous CERES and MODIS retrievals were used for the evaluation of the mean daily shortwave aerosol radiative budget (SWARF) and of the mean daily surface albedo change radiative forcing (LURF) during the peak of the biomass burning season (August to September) from 2000 to 2009.

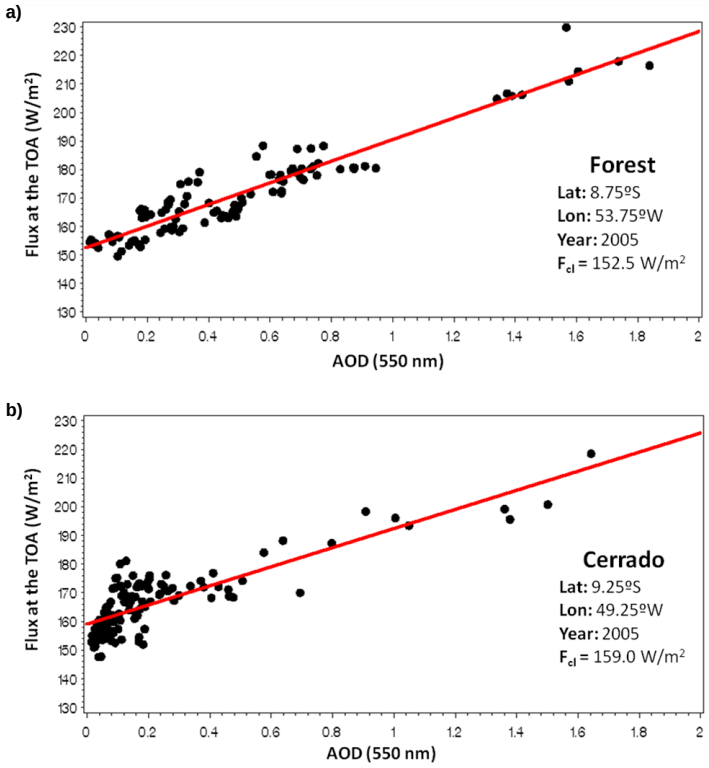

Fig. 4. Examples of the linear fit of CERES flux at the TOA versus MODIS AOD at 550 nm for two 0.5° × 0.5° cells located at areas covered by **(a)** forest and **(b)** cerrado.

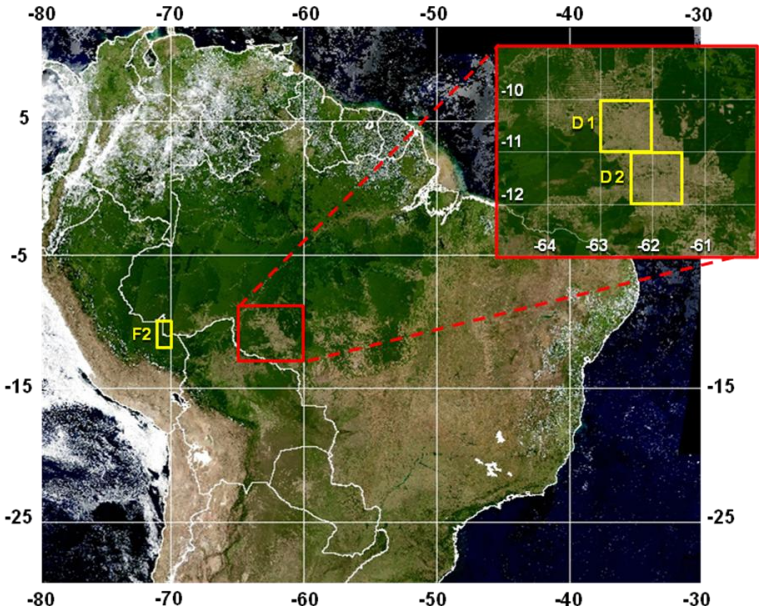

Fig. 5. Areas selected in South America for the surface albedo change radiative forcing evaluation (LURF). The yellow squares correspond to the deforested areas (D1 and D2) and forested (F2) areas selected.

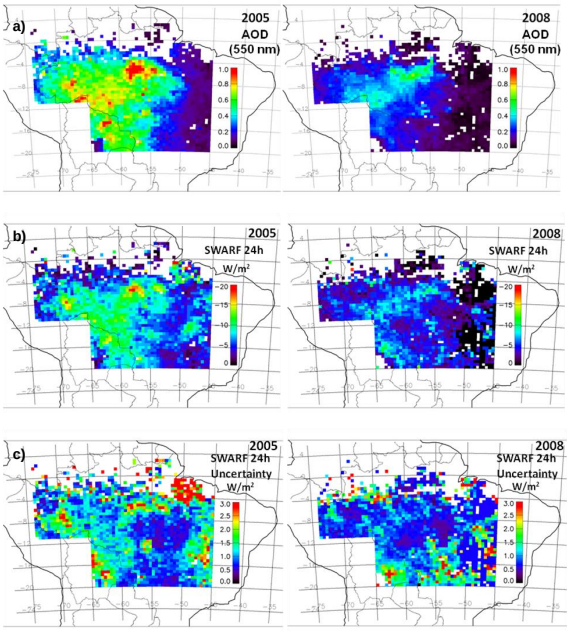

Fig. 6. Average spatial distributions during the peak of the biomass burning season of the: **(a)** aerosol optical depth retrieved by MODIS sensor onboard Terra satellite; **(b)** mean daily aerosol direct radiative forcing ($SWARF_{24h}$) and **(c)** estimated uncertainty of the $SWARF_{24h}$ for the years 2005 (left) and 2008 (right). To estimate the uncertainty of $SWARF_{24h}$ the uncertainty of the points in each $0.5^{\circ} \times 0.5^{\circ}$ cell was estimated by setting the reduced chi-squared equal to 1. The covariance between the flux for clean conditions (F_{cl}) and the mean polluted flux observed during the studied period was also considered in this calculation.

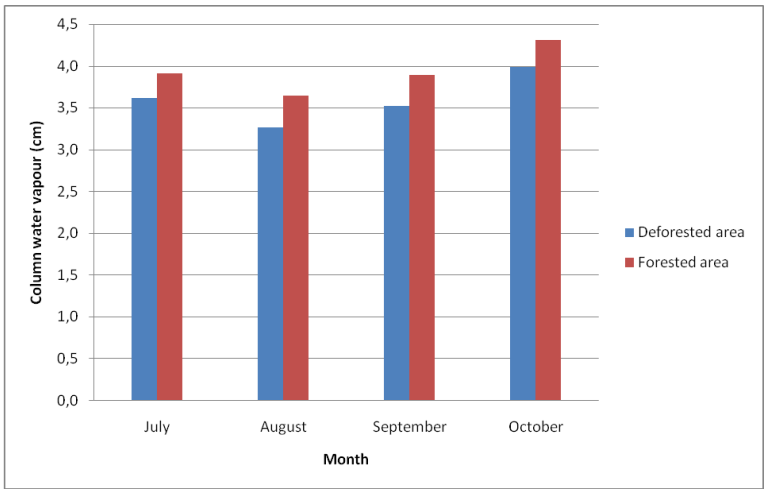

Fig. 7. Column water vapour content retrieved by AERONET sunphotometers at a deforested area (located at 10.76° S, 62.36° W) and a forested area (located at 10.08° S, 61.93° W) from July to October 2002.

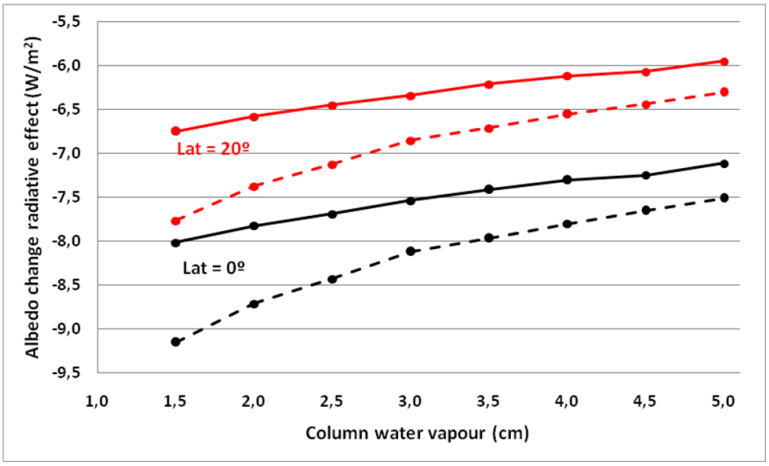

Fig. 8. Albedo change radiative effect as a function water vapour amount in the atmosphere before deforestation. Black and red lines indicate the results over sites located at latitude = 0° and at latitude = 20°, respectively. Solid lines represent the effect considering equal water amounts before and after deforestation. Dashed lines represent the effect considering the deforested region is 0.35 cm drier after deforestation.